Received: 7 July 2021 | Revised: 4 August 2021 | Accepted: 29 August 2021

DOI: 10.1111/jace.18119

Journal of the American Ceramic Society

ORIGINAL ARTICLE

# Flash sintering and dielectric properties of $K_{0.5}Na_{0.5}NbO_3$

İlyas Şavklıyıldız[1] | Çiğdem Okur[1] | E. Koray Akdoğan[2]

[1] Department of Metallurgical and Materials Engineering, Konya Technical University, Konya, Turkey

[2] Department of Materials Science and Engineering, Rutgers University, Piscataway, New Jersey, USA

**Correspondence**
İlyas Şavklıyıldız, Department of Metallurgical and Materials Engineering, Konya Technical University, Konya, Turkey.
Email: isavkliyildiz@ktun.edu.tr

**Funding information**
the Scientific Research Projects Coordination Unit (SRPCU) of Selçuk University, Grant/Award Number: 18401032; the Scientific Research Projects at Konya Technical University, Grant/Award Number: 191019035

## Abstract

$K_{0.5}Na_{0.5}NbO_3$ (KNN) of 4-$\mu$m average particle size was flash sintered in parallel plate capacitor configuration (PPCC) under 100 V/mm (0.8 mA/mm$^2$ cut-off) with 10°C/min heating rate in air. Precipitous densification occurred from $T_f$ = 662–670°C ($T_f$–furnace temperature) in 60 s with 55 mW/mm$^3$ peak power absorption at $T_f$ = 667°C, resulting in 98% dense ceramic of < 5-$\mu$m grains size. No grain growth was observed. A cubic grain morphology was inherited from the starting KNN powder. No sign of liquid phase formation on grain boundaries (GBs) was detected. A 147°C rise above $T_f$ = 667°C due to Joule heating is predicted. At 25°C and 1 kHz, relative permittivity ($\varepsilon_r$) and dielectric loss (tan($\delta$)) are 4096 and 2.9%, respectively. From 0.1 to 100 kHz, $\varepsilon_r$ and tan($\delta$) undergo relaxation, reaching $\varepsilon_r$ = 577 and tan($\delta$) = 0.2% at 1000 kHz. Variation of $\varepsilon_r$ with temperature revealed Amm2 → P4mm and P4mm → Pm3m transitions at ~204°C and 409°C, respectively. As per Curie–Weiss analysis, Curie temperature and Curie–Weiss constant are $\theta$ = 375°C and $C = 3.1 \times 10^{-5}$°C for the P4mm → Pm3m transition, respectively. The transition is first order as $T_{tr} > \theta$ with a diffusiveness exponent $\gamma$ = 1.04, indicating normal ferroelectric behavior. The low-frequency dielectric relaxation is attributed to the space charge in the vicinity of GBs, which is a remnant of flash sintering. Joule heating cannot alone account for the densification in 60 s, which we substantiate within the framework of phase equilibrium and diffusion kinetics. We conjecture that oxygen vacancies start ionizing at $T_f$ = 662°C, couple with the applied electric field via the Lorentz force, and increase their electrochemical potential, causing ultrafast densification. The effects of sample shape, size, and PPCC contributing to high sintered density are also discussed.

KEYWORDS
dielectric relaxation, ferroelectric, flash sintering, KNN, permittivity, sintering, space charge

## 1 | INTRODUCTION

Among all lead-free piezoelectric ceramics, sodium potassium niobate, $(K_{0.5}Na_{0.5})NbO_3$ (KNN), and its compositional variations exhibit enhanced permittivity and high transition temperature.[1-3] The ferroelectric polymorphs in the KNN system are the orthorhombic (Amm2) and tetragonal (P4mm) phases.[4,5] When KNN forms ternary systems such as $(K_{0.44}Na_{0.52}Li_{0.04})(N_{b0.84}Ta_{0.1}Sb_{0.06})O_3$, the Amm2 and P4mm phases coexist due to morphotropic phase boundary formation, which leads to high piezoelectric properties.[6–8] KNN ceramics and their solid solutions with various other lead-free perovskites make them primary candidates for microwave devices, piezoelectric

  

sensors and actuators, and ferroelectric random-access memories, to name a few.[1] On the other hand, the volatile alkaline species in KNN pose difficulties in stoichiometric control at high temperatures during sintering.[5] Furthermore, KNN ceramics are susceptible to moisture.[9] Sintering aids such as $MnO_2$[10] or electric field–assisted sintering techniques such as spark plasma sintering were proposed for counteracting the aforementioned difficulties associated with sintering of KNN ceramics and its variations.[11]

The flash sintering (FS) method enables one to rapidly sinter a ceramic preform (a.k.a. green body) at temperatures that are typically 50% less than the conventional sintering temperature[12,13] while reducing the sintering time by 1 to 3 orders of magnitude.[14–17] The viability of the FS method was demonstrated for many materials.[14–18] Typically, a dc electric field is applied to a given material (insulator or semiconductor) in the green state (as-pressed powder compact) while it is heated at a fixed heating rate in the FS method.[14–17] At a certain temperature, the specimen's electrical conductivity precipitously increases and is accompanied by extremely rapid mass transport.[14–17] Under such conditions, the ceramic undergoes ultrafast densification, the root causes of which are still under investigation.[14–17] Several mechanisms were conjectured including the formation of field-induced vacancies and Frenkel pairs, excessive localized joule heating, among others.[14–17] Cologna and colleagues[14–17] provide a detailed account of the various mechanisms proposed to explain FS and discuss major results thereto appertaining. Furthermore, an anomalous unit cell expansion, which correlates with the precipitous densification during FS, was reported in an in situ ultrarapid synchrotron x-ray diffraction study for yttria-stabilized zirconia.[19]

Several research groups have already reported on the sintering of KNN by classical means.[10–13] Typically, KNN is sintered in air at 1000–1200°C under some ad hoc stoichiometric control[10–13] A reactive-flash process was proposed for producing single-phase KNN from an equimolar mechanical mixture of $KNbO_3$ and $NaNbO_3$.[20,21] Such studies showed the possibility of FS KNN ceramics (dog bone specimen shape) in 30 s at 990°C to 94 % theoretical density under 50 V/cm and 20 $mA/mm^2$.[20] A core-shell structure was postulated to form that is based on Na and K, leading to preferential heating at particle surfaces and Na volatilization.[22] Recently, current flow through grain boundaries (GBs) was proposed as the governing mechanism for FS of KNN, causing amorphization and particle sliding.[22] However, there is no consensus on how FS occurs in KNN in particular, as is the case for a plethora of other ceramics.[21,23–25] Above all, there are no reports of FS of KNN that resulted in sintered density well above 95%.

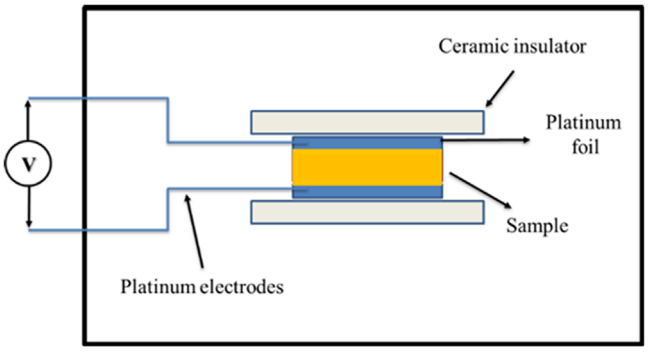


**FIGURE 1** Schematic of the flash sintering (FS) system developed for this study. FS of $K_{0.5}Na_{0.5}NbO_3$ (KNN) is accomplished in the parallel plate capacitor configuration (PPCC). The PPCC enables one to apply the electric field uniformly, leading to homogenous densification

In this study, we will demonstrate the FS of KNN at lower furnace temperatures and shorter sintering times by applying an electric field to the specimen in the parallel plate capacitor configuration (PPCC). Our approach enables us to induce a homogenous flash in the ceramic, which leads to uniform sintering of KNN to high density. We also present results on the dielectric properties of flash sintered KNN in the 100 Hz-1 MHz range. In addition, we provide a full Curie–Weiss analysis on the ferroelectric (P4mm) → paraelectric (Pm3m) transition that is based on the temperature dependence of permittivity at 1 kHz.

## 2 | EXPERIMENTAL

The KNN powder was synthesized by the conventional solid-state method. Stoichiometric amounts of commercial sodium carbonate $Na_2CO_3$ (Sigma–Aldrich, 99.5%), potassium carbonate $K_2CO_3$ (Merck, 99.0%), and niobium oxide $Nb_2O_5$ (Alfa Aesar, 99.9%) were ball-milled for 12 h in ethanol ($C_2H_5OH$) using zirconia ($ZrO_2$) grinding media. The milled powder was calcined at 800°C for 2 h and then re-milled for another 10 h. The KNN powder, which was of 4-$\mu$m average particle size, was mixed with 5 wt% polyethylene glycol ($C_2H_6O_2$) prior to the uniaxial pressing of discs. The powder was then pressed uniaxially in a hardened stainless steel die into discs of 13-mm diameter and 1.5-mm thickness under a pressure of 200 MPa. Binder removal was accomplished at 500°C for 1 h (heating rate 1°C/h). The density after binder removal, which we determined geometrically, was 63%.

The experimental setup that we used for FS is illustrated in Figure 1. The disc-shaped KNN specimen was positioned in the PPCC as explained in detail elsewhere.[19,26] Both faces of the specimens were brought in contact with platinum (Pt) foils to establish ohmic contacts, enabling us

to apply the electric field for FS thereby. The Pt foils were attached to Pt wires, which, in turn, were connected to the direct current (dc) power source. The sample was then sandwiched between ceramic insulators to ensure good contact between the foil and sample. The furnace temperature was increased with a heating rate of 10°C/min. The furnace temperature was measured by a thermocouple that was positioned 5 mm away from the specimens' lateral surface. A dc electric field of 100 V/mm was applied to the sample with a digital power source (Sorenson XG 1500). The current cut-off value was set to 0.8 mA/mm$^2$ with the purpose of minimizing joule heating and preventing thermal runaway.

Voltage and current values were recorded as a function of time instead of temperature because current draw by the sample could have caused joule heating, raising the internal temperature of the specimen above the furnace temperature thereby.

The density of the flash sintered samples was measured by the Archimedes method. Field emission scanning electron microscopy (FE-SEM, Hitachi SU5000) was used to assess the degree of densification, microstructure, and the level of porosity. An x-ray diffractometer (Rigaku ZSX Primus-II XRD) was used for qualitative phase analysis of flash sintered KNN samples.

An inductance-capacitance-resistance (LCR) meter (Hioki IM3536) was used to measure the relative permittivity ($\varepsilon_r(\omega)$) and loss tangent ($\tan\delta(\omega)$) as a function of frequency ($\omega$ = 100 Hz–1000 kHz; $\omega$ frequency) at 298 K by measuring the capacitance as per von Hippel.[27]

$$\varepsilon(\omega) = C(\omega)\left(\frac{t}{A\varepsilon_o}\right), \quad (1)$$

where $t$ is the sample thickness, $A$ is the electrode area (surface area of the sample in this study), and $\varepsilon_o$ is the permittivity of free space ($8.854 \times 10^{-12}$ F/m).[27] The $\tan(\delta(\omega))$ was directly obtained from the LCR meter, which is defined by the complex permittivity $\varepsilon_r(\omega) = (1/\varepsilon_o)[\varepsilon'(\omega)\text{-}j\varepsilon''(\omega)]$ as per von Hippel.[27]

$$\tan(\delta(\omega)) = \left|\frac{\varepsilon''(\omega)}{\varepsilon'(\omega)}\right|, \quad (2)$$

where $\varepsilon'(\omega)$ and $\varepsilon''(\omega)$ are the real and imaginary parts of the complex permittivity, respectively, and $j^2 = -1$. The $\varepsilon_r$ was also determined as a function of temperature at 1 kHz to assess the phase transitions in flash sintered KNN and to carry out Curie–Weiss analysis[28,29] (see Section 3.3). The surfaces of flash sintered KNN samples were polished, and then silver paste was applied onto them to form good ohmic contacts for dielectric property measurements. The silver paint was cured for 1 h at 400°C.

# 3 | RESULTS AND DISCUSSION

## 3.1 | Electric field-current relations in FS of KNN

Figure 2 depicts the variation of the electric field, current density, and power density as a function of time while KNN was heated with 10°C/min heating rate under an electric field intensity of 100 V/mm.

Initially, we observed no current draw until $T_f$ = 662°C was reached, suggesting that KNN was in the insulator state for 25°C < $T_f$ < 662°C under 100 V/mm. In other words, an electric field of 100 V/mm was insufficient to drive a current through the 63% dense KNN powder compact. As such, we concluded that the electrical conductivity of KNN was not sufficiently high in the 25°C < $T_f$ < 662°C interval. A leakage current of 0.016 mA/mm$^2$ was recorded when $T_f$ reached 662°C. Further increase in temperature caused an increase in the current to 0.24 mA/mm$^2$ in 30 s. Thereafter, the sample showed a precipitous increase in current, reaching the current density cut-off (0.8 mA/mm$^2$) at $T_f$ = 667°C in 5 s. At $T_f$ = 667°C, the power source switched from voltage control to current control so as to prevent the current from exceeding the pre-set current density cut-off. Specifically, the dc power source reduced the electric field to 18 V/mm to maintain a constant current density of 0.8 mA/mm$^2$ as intended. However, it took an additional 20 s for the electric field to stabilize in the range $T_f$ = 667–670°C (see Figure 2). First, the electric field fluctuated around 18 V/mm. Second, it spontaneously stabilized at 4.7 V/mm, causing fluctuations around the pre-set current density (0.8 mA/mm$^2$) to vanish (see Figure 2). At the end of the fluctuations, the transient current-voltage response of KNN switched over to a steady-state response. Prolonged dwelling in the steady state would have led to Joule heating, which is to be avoided since it is known to cause abnormal grain growth.[30,31] As such, the power was cut off once the current density stabilized at 0.8 mA/mm$^2$ at which point $T_f$ = 670°C. We attribute the fluctuations in current density around the pre-set value (0.8 mA/mm$^2$) to defect processes associated with the formation of GBs from particle-particle contacts. Moreover, we consider the 20 s spanning from 667–670°C as part of the FS process for KNN as it leads to a stable electrical conductivity that is expected from a highly dense polycrystalline solid. From the foregoing, we also conjecture that the space charge settles to its equilibrium configuration in the 667–670°C interval within 20 s.

Figure 3 shows a real-time image of a representative KNN specimen that was flash sintered in this study. Specifically, the photo depicts the instant at which the

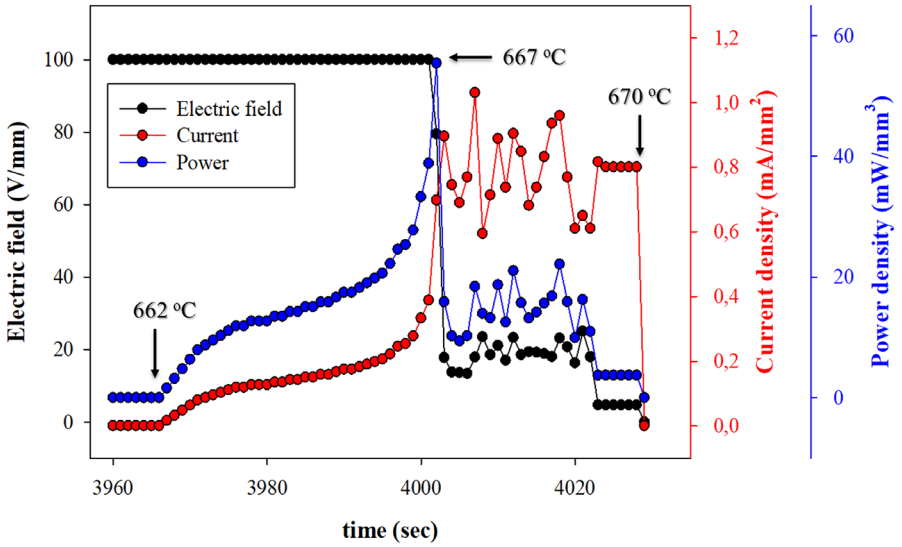


**FIGURE 2** The time evolution of current and power density under 100 V/mm electric field strength and with 10°C/min heating rate that was observed in FS of KNN. The current cut-off was pre-set to 0.8 mA/mm$^2$. A sintered density of 98% was reached in 60 s as the furnace temperature varied from 662 to 667°C

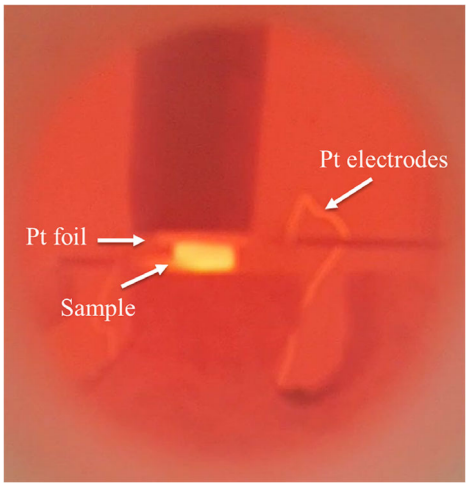


**FIGURE 3** The real-time image depicting the instantaneous flash (electroluminescence) in KNN at 667°C furnace temperature ($T_f$). The flash lasted ≤ 5 s. The current drawn by KNN at $T_f$ = 667°C under 100 V/mm is 0.8 mA/mm$^2$ (cut-off) corresponds to a peak power absorption of 55 mW/mm$^3$

specimen flashed. This is a well-documented electroluminescence phenomenon,[32–35] and in our case, it occurred as $T_f \rightarrow$ 667°C while the current draw by the KNN specimen reached 0.8 mA/mm$^2$. The instantaneous volumetric power absorption ($W$) by the KNN specimen accompanying the uniform flash was 55 mW/mm$^3$ ($W = [(iV)/\psi]$, where $i$ is the current, $V$ the voltage, and $\psi$ is the specimen volume. Hence, the FS parameters (electric field magnitude, current limit (cut-off), the PPCC, specimen geometry specimen size) that were chosen for this study have proven to be effective as they insured a homogenous power absorption by the specimen. Such power absorption is a fundamental prerequisite for homogenous densification in FS of ceramics.[36]

The sintered density of flash sintered KNN, as measured by the Archimedes' method, was determined as 98% of the x-ray density. The sintered density that was obtained in this study (98%) compares favorably with conventionally sintered KNN of ~95% and to prior studies on FS of KNN to ~92%.[37–39] Most importantly, FS was accomplished at $T_f$ = 667°C ( $T^{\otimes}$ = 809°C, see Section 2) in 60 s in this study, which is in stark contrast to conventional sintering of KNN requiring up to 6 h at 1000 < $T$ < 1200°C.[37–39] Furthermore, the FS temperature, which we report as $T_f$ = 667°C in our study, is approximately 300°C lower than previously reported $T_f$ in KNN FS studies.[40,41] We attribute the lower FS temperature and shorter sintering time to the PPCC and the specimen geometry (thin disc with high diameter to thickness ratio; see Section 2) that we implemented in this study. The said PPCC enables one to apply a higher electric field (100 V/mm) to the specimen uniformly. The magnitude of the applied electric field ensures sintering at low furnace temperatures to high density.[42] On the other hand, the uniformity of the applied field produces a uniform flash, resulting in a uniform microstructure (see Section 3.3).

## 3.2 | Joule heating considerations

The amount of power absorption by the ceramic is important for gaining insight into the mechanism(s) governing FS.[16,43–48] One of the top contenders for the governing

mechanism in FS, which remains to be conclusively proven, is Joule heating.[16,43–48] The main hypothesis of the Joule heating mechanism is that the true specimen temperature (at particle-particle contacts or otherwise) diverges from the furnace temperature and reaches temperatures close to the melting temperature (solidus temperatures more precisely) with the possibility of local melting.[17,45–49] Consequently, it is further hypothesized that very high diffusion fluxes become accessible since thermal activation is very high due to Joule heating (the formation of a liquid phase would also enhance the diffusion kinetic substantially).[17,45–49] While some Joule heating is unavoidable, we did not expect excessive Joule heating (thermal runaway) in our FS work of KNN because of the following reasons: (i) the cut-off current density was relatively low, (ii) the PPCC keeps the specimen in contact with Pt foil, enabling heat transfer from the specimen to the surroundings by conduction in addition to radiation. The heat transfer via conduction ($\Psi_c$) is related to the specimen thickness ($h$) as $\Psi_c \sim 1/h$,[47] (iii) the large surface to volume ratio of the specimen (thin disc geometry) enables faster heat transfer to the surrounding as per Fourier's first law,[50] and (iv) the transient nature of the implemented FS protocol, which prevented the specimen from entering steady-state conditions in terms of the current flow. Despite the foregoing reasoning, we computed the sample temperature using the blackbody radiation model given by[21,32–35]

$$T^{\otimes} = T_f \left[1 + \frac{W}{\Xi T_f^4}\left(\frac{\Omega}{\Lambda}\right)\right]^{\frac{1}{4}}, \tag{3}$$

where $T^{\otimes}$ is the specimen temperature, $T_f$ is the furnace temperature (ambient), $W$ is the volumetric power absorbed by the specimen, $\Xi$ is the blackbody radiation constant ($5.67 \times 10^{-8}$ W/(m$^2$K$^4$)), and $(\Omega/\Lambda)$ is the volume-to-surface ratio of the specimen in question. The result indicated $T^{\otimes} = 809$°C, which corresponds to an increase in the specimen temperature by 147°C. The instantaneous peak temperature ( $T^{\otimes} = 809$°C), which was reached in 60 s when $T_f$ increased from 662 to 667°C, is clearly not sufficient to account for the ultrarapid densification of KNN in 60 s. Typically, KNN is sintered isothermally in the range $1000 < T < 1200$°C for 1–6 h to obtain acceptable densification.[10–13,51] A similar conclusion was reported in a finite element study on KNN where it was shown the temperature rise at particle-particle contact was not high enough to induce ultrafast densification.[36,52] Hence, we conclude Joule heating is present and unavoidable in the FS of KNN under the conditions of this study, while it cannot solely account for the observed densification to 98%. In other words, the densification kinetics of FS in KNN are not only driven by thermal activation. We will further elaborate on thermal runaway and such in relation to the $KNbO_3$-$NaNbO_3$ phase diagram in what follows.

## 3.3 | Microstructure and phase analysis of flash sintered KNN

Figure 4 depicts representative FESEM micrographs of flash sintered KNN ceramic surfaces, which were obtained in this study. As depicted in Figure 4A, the observed microstructure is that of a highly dense polycrystalline ceramic that agrees with the measured 98% density by the Archimedes method. The grains in the flash sintered KNN are cubic in shape, which is the same shape as that of the particles comprising the KNN powder used in this study (the typical powder morphology for KNN is cubic).[53,54] Therefore, FS of KNN with 100 V/mm at $T_f = 667$°C and 0.8 mA/mm$^2$ current density cut-off did not change the initial particle shape (not shown) during densification. Normally, the grain shape would change to flat GBs during sintering and form triple junctions of 120° dihedral angles, reaching stable equilibrium in the polycrystalline state (metastable with respect to single crystal state, of course) as per surface thermodynamics.[23,55–57] However, this is not the case here, which indicates the microstructure of flash sintered KNN is metastable in the sense indicated above. Figure 4B shows a representative microstructure at a higher magnification where one observes a median grain size that is $< 5\,\mu$m, which means no grain growth occurred as stated earlier (the starting particle size of KNN was ~4 $\mu$m as mentioned in Section 2). We attribute the lack of grain growth to the FS protocol of this study, which did not allow the system (the KNN ceramic) to enter steady state under 100 V/mm at 670°C. In so doing, grain growth was suppressed.[24,25] By using image analysis on Figure 4B and other representative high-resolution images (not shown), the flash sintered density of KNN was re-assessed as 98.5%. Hence, the density, which was measured as 98% using the Archimedes method, was confirmed.

A closer look at the flash sintered microstructure of KNN (see Figure 4C as a representative microstructure) shows no sign of local melting on GBs (formerly particle-particle contacts), which rules out excessive Joule heating during the FS of KNN in this study. The $KNbO_3$-$NaNbO_3$ binary system is isomorphous,[58] in which an equimolar KNN solution has a solidus temperature of ~1175°C. In the event of excessive Joule heating to a temperature near the solidus, one would expect the highest diffusivity for the rate-limiting species, causing a substantial reduction in sintering time. On the other hand, if the rise in temperature were in excess of ~1175°C, one would expect the formation of a liquid phase that is rich in $KNbO_3$ (at $1175^+$°C the composition of the first liquid formed

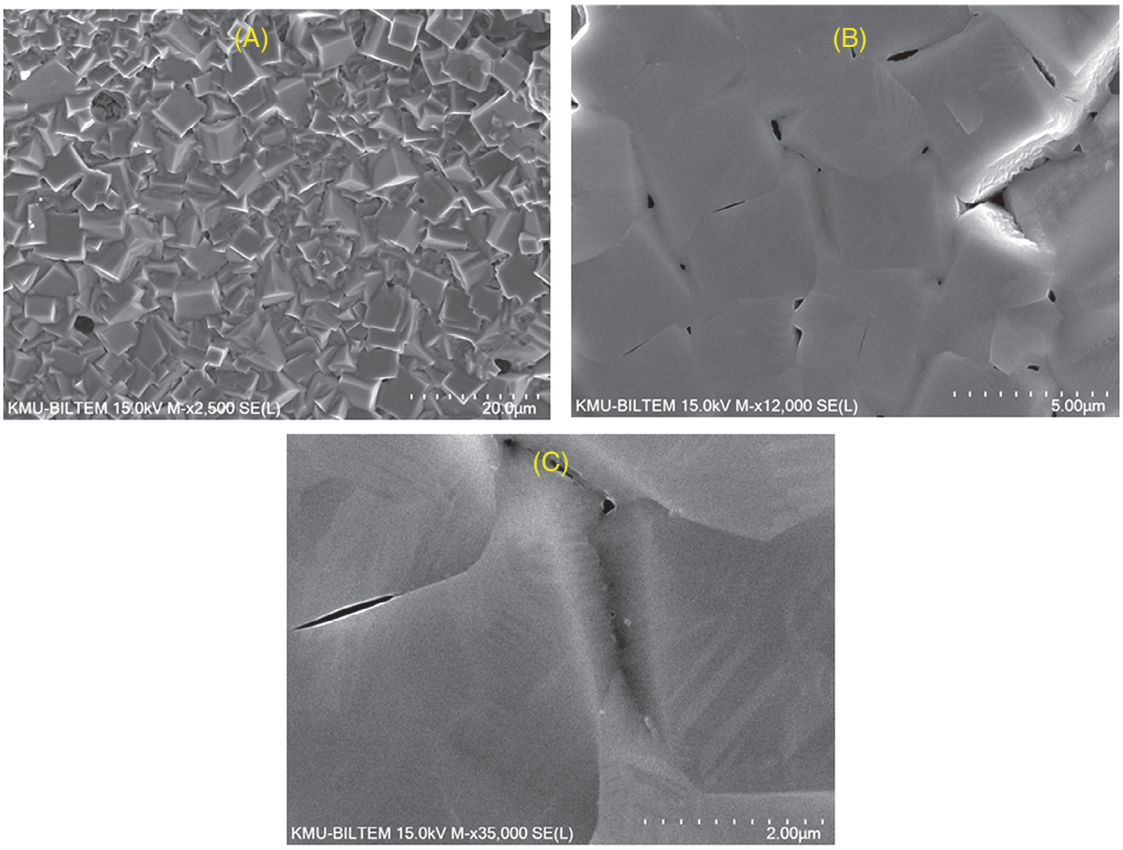


**FIGURE 4** Field emission scanning electron microscopy images showing the microstructure of flash sintered KNN at $T_f = 667°C$ under 100 V/mm with 0.8 mA/mm$^2$ cut-off: (A) x2500 magnification showing a densely sintered microstructure that is comprised of cubic grains; (B) x12 000 magnification showing residual porosity that is mostly situated on grain boundaries (GBs). The shape of the grains is cubic with flat interfaces. (C) x35 000 magnification showing no secondary phases on GB. No signs of melting at GB observed, suggesting no excessive Joule heating occurred at particle-particle contacts during FS

upon heating is approximately $0.95KNbO_3$-$0.05NaNbO_3$ [58]; here + "larger than … by a very small fraction") under conditions of near equilibrium. The $KNbO_3$-rich liquid phase would, in principle, provide easy diffusion via the mass transport coefficient of the rate-limiting species.[59] In other words, FS of KNN would become transient liquid phase sintering at temperatures above 1175°C in principle.

Although the foregoing considerations appear to be very compelling at first, we note that conventional sintering of KNN in the temperature range 1000–1200°C under isothermal conditions typically takes 1–6 h. This is in stark contrast with the 60 s it took to flash sinter KNN (4-$\mu$m particle size) at $T_f = 667°C$, under 100 V/mm, and with 0.8 mA/mm$^2$ as the current limit. The reduction in sintering time is approximately 1 order of magnitude. Therefore, the time scale differential between conventional sintering of KNN based on solid-state diffusion and FS of KNN (as described in this study) makes excessive Joule heating to the vicinity of the sub-solidus temperature ($\sim <$ 1175°C) highly improbable as a viable hypothesis.

For the liquid phase–assisted FS of KNN scenario (> 1175°C) to gain traction, one needs to assume the following: (i) the solid (the KNN compact) will never be in the superheated state as the temperature shoots above the solidus temperature for a few seconds, and melting is instantaneous, (ii) upon current cut-off at $T_f = 667°C$, the flash sintered (dense) KNN will cool under near-equilibrium conditions so that the aforementioned liquid phase ($0.95KNbO_3$-$0.05NaNbO_3$) will re-dissolve in solid KNN to restore the nominal composition and its homogeneity. First, the specimens were cooled to room temperature (RT) under zero field and at the natural cooling rate of the furnace in the FS study on KNN considered herein, which is certainly not equilibrium cooling. Second, we have not observed residual second phases (see ensuing discussion and Figure 5). Third, we have not observed a clear indication of melting at particle contacts that would have altered the grain morphology and grain size. Finally, sintering times were reported for conventional sintering of KNN at $T >$ 1175°C is on the order of 1 h. Hence, we are once again led to conclude that Joule heating by itself

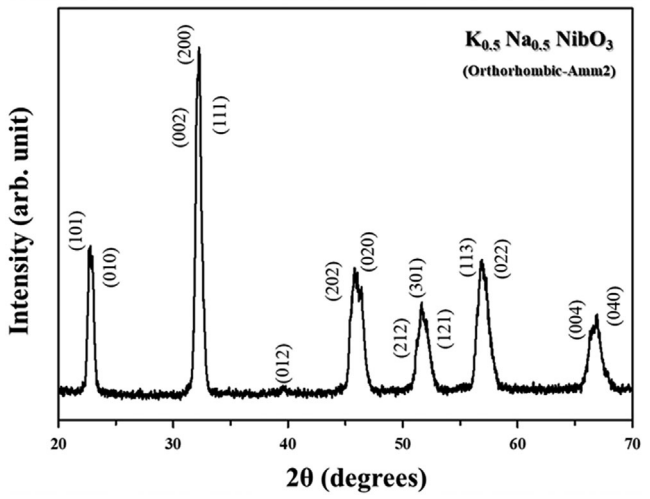


**FIGURE 5** Indexed diffraction pattern of flash sintered KNN at room temperature. The flash sintered ceramic is single phase. The unit cell crystal class is orthorhombic with base-centered space group Amm2 (38). The observed diffraction pattern matches with PDF card number (01-084-6855)[52]

cannot account for the observed ultrafast densification at $T_f = 667°C$.

Figure 4C also reveals flat GBs with no grain growth and change in GB curvature that is otherwise typical of long-range mass transport during sintering.[23,55–57] Here, we observe GB formation at particle-particle contacts where two flat and parallel particle faces came into contact during FS (see Figure 4B,C). In fact, it appears as if the cube-shaped KNN particles were stuck on top of each other. This, in turn, leads us to conjecture that FS occurred by local diffusion fluxes over short distances across particle-particle contact areas. The evolution of the pores (voids) depicted in Figure 4B,C, which are situated on the GBs, could be due to two mutually exclusive mechanisms: (i) lack of full particle-to-particle contact at those locations in the as-pressed state prior to sintering, which is common in green bodies, and (ii) vacancy clustering during FS. The origins of the aforementioned porosity phenomena are beyond the scope of this study, but it suffices to indicate that the diffusion flux provided by FS in this study was not sufficient to fill the pores, removing the residual porosity (~2%) thereby.

Several studies reported that some materials could undergo polymorphic or transient phase transformations during FS.[60,61] KNN has two known polymorphic phase transitions (Amm2 → P4mm and P4mm → Pm3m) over the temperature range of interest (25–700°C).[4] Hence, we carried out qualitative x-ray diffraction (XRD) phase analysis to ascertain the effects of FS, if any, on the phase equilibria in the KNN system. Figure 5 depicts the XRD spectrum of flash sintered KNN that we indexed using Powder Diffraction File (PDF) 71–0946. The flash sintered KNN at room temperature was found to be single phase, belonging to the orthorhombic space group Amm2. As such, FS with 100 V/mm and 0.8 mA/mm$^2$ current density cut-off has no effect on phase equilibria in the KNN system. We will comment on the sequence of phase transitions in KNN with increasing temperature in Section 3.4.

## 3.4 | Dielectric properties of flash sintered KNN

Figure 6A shows the frequency dependence of relative dielectric permittivity ($\varepsilon_r$) and dielectric loss tangent (tan($\delta$)) in the frequency range of 0.1–1000 kHz for KNN. The $\varepsilon_r$ is 4096 while tan($\delta$) is ~2.9% at 1 kHz. The flash sintered KNN in this study has a reasonable $\varepsilon_r$ (at 1 kHz) as compared to the ones reported earlier in the literature on KNN.[34–38] Over the 1–100 kHz range, there is pronounced relaxation in $\varepsilon_r$ and tan($\delta$) from 4096 to 557 and from 2.9% to 0.8%, respectively. Beyond 100 kHz, $\varepsilon_r$ shows negligible frequency dependence while tan($\delta$) decreases further to 0.2% at 1000 kHz. Such dielectric relaxation over the 1–1000 kHz range is a well-known phenomenon in cubic perovskite-type materials such as $CaCu_3Ti_4O_{12}$ and in $BaTiO_3$-based ferroelectric boundary layer capacitors (BLC).[62–64] The BLC phenomenon is customarily analyzed by the Maxwell–Wagner model.[27]

In BLCs, the GBs act as capacitors of low capacitance that are in series with the capacitance of the grains, resulting in a very high effective capacitance for a given polycrystalline ferroelectric ceramic.[65–68] It follows from the foregoing line of reasoning that $\varepsilon_r = 577$ at 100 kHz represents the average relative permittivity of the KNN grains since the BLC effect is relaxed out at that frequency. On the other hand, $\varepsilon_r = 4096$ at 1 kHz represents the effective average relative permittivity of the polycrystalline KNN to which the GBs make a large contribution because of their space charge capacitance. Here, we use the term space charge in its broadest sense to indicate the distribution of charge in the vicinity of the GBs due to whichever defects are present in the polycrystalline ceramic of interest.[21,69–71] The BLC effect in $BaTiO_3$-based capacitors is due to the loss of oxygen[50] in reducing atmospheres during sintering, resulting in GB space charge that is associated with oxygen vacancies.[72] In stark contrast, FS of KNN was carried out under ambient conditions, which precludes any possibility for reduction as air is an oxidizing medium. While one cannot rule out the creation of oxygen vacancies due to an applied electric field completely,[73] what is of central importance is the enhanced diffusivity of oxygen vacancies under superimposed thermal and electric fields in FS. That is so because mass transport in oxide ceramics such as

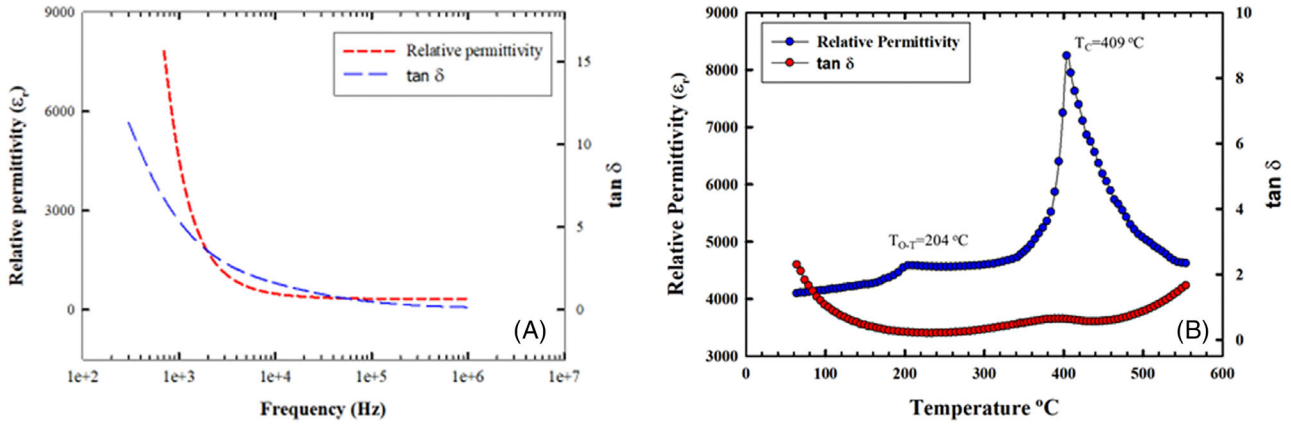


**FIGURE 6** Dielectric properties of KNN of 98% density: (A) variation of the relative permittivity ($\varepsilon_r$) and loss tangent (tan($\delta$)) in the range 0.1–1000 kHz, showing a pronounced relaxation in $\varepsilon_r$ that is attributed to space charge relaxation at GB; and (B) temperature dependence of $\varepsilon_r$ and tan($\delta$) in the range RT-560°C at 1 kHz. The orthorhombic (Amm2) → tetragonal (P4mm) and tetragonal (P4mm) → cubic (Pm3m) phase transitions were observed at 204°C and 409°C, respectively. The relative permittivity and loss tangent at 409°C are $\varepsilon_r^{max} = 8246$ and tan($\delta$) = 0.8%, respectively

KNN is known to occur by oxygen vacancy diffusion.[69,74] Oxygen vacancies can couple with the applied electric field (in addition to the thermal activation) via the electrochemical potential ($\mu^*$) of oxygen vacancies ($V_o$) as per Guggenheim.[75,76]

$$\mu^*_{V_o} = \left[\mu^{\odot}_{V_o} + k_B N_A T \ln(a_{V_o})\right] + \eta_{V_o} F \xi_{V_o}, \qquad (4)$$

where the term in the square brackets is the chemical potential of oxygen vacancies ($\mu^{\odot}_{V_o}$: chemical potential of oxygen vacancies in their standard state; $k_B$: Boltzmann constant; $N_A$: Avogadro's number; $a_{V_o}$: activity of oxygen vacancies) and $\eta_{V_o} F \xi_{V_o}$ is the local electrostatic potential energy associated with the oxygen vacancies. Here, $\xi_{V_o}$ is the local voltage (equivalently the Lorentz field or local field)[27] acting on the oxygen vacancy due to an applied electric field, $F$ is the Faraday constant, and $\eta_{V_o}$ is the charge carried by the oxygen vacancy if oxygen vacancies are ionized. Hence, $\xi_{V_o}$ can be extremely high with a sufficiently high applied electric field, resulting in $\eta_{V_o} F \xi_{V_o} >> [k_B N_A T \ln(a_{V_o})]$. As such, the diffusive flux of oxygen vacancies $J_{V_o}$ can be greatly enhanced by the coupling of the applied electric field with charged oxygen vacancies via $\xi_{V_o}$ since $J_{V_o} \propto -\nabla\mu^*_{V_o}$ where $\nabla\mu^*_{V_o}$ is the driving force of $J_{V_o}$.[77] The foregoing analysis is valid if and only if the oxygen vacancies carry a charge (single or double) at a given temperature so that $\eta_{V_o} \neq 0$ ( $\eta_{V_o} = 1$ or 2 depending on the degree of ionization). In other words, the gradient of $\xi_{V_o}$ is the Lorentz field ($-\nabla\xi_{V_o} = \Phi$)[78] to which corresponds the Lorentz force ($\Psi$) via $\Xi = \eta_{V_o}\Phi$.[78] The Lorentz force, which is responsible in displacing oxygen vacancies, is nonzero if and only if $\eta_{V_o} \neq 0$. Since FS of KNN under 100 V/mm at $T_f = 667$°C resulted in 98% density in 60 s, we infer that the applied field has induced the necessary $J_{V_o}$ by mobilizing oxygen vacancies due to the Lorentz force while the system was heated at 10°C/min. Consequently, we postulate $T_f = 662$°C as the temperature at which oxygen vacancies start to couple with the applied electric field in the aforementioned fashion, contributing to if not chiefly causing rapid densification. We also postulate the space charge governed ultrahigh permittivity, which was observed at 1 kHz, is a remnant of FS. We note that conventionally sintered KNN in air, which relies on thermal activation alone, does not undergo a pronounced dielectric relaxation as flash sintered KNN does.[79–81] In other words, the space charge relaxation is much more pronounced in flash sintered KNN than conventionally sintered KNN. In fact, the space charge relaxation is FS's residual imprint in KNN based on what was observed in this study.

Figure 6B depicts the temperature dependence of $\varepsilon_r$ and tan($\delta$) over the temperature range 25–500°C (the span from 300–500°C is shown for clarity) at 1 kHz, which enabled us to determine the phase transitions between the ferroelectric phases (FE → FE), and from the FE → PE (paraelectric) phase in flash sintered KNN. Specifically, we observed the FE (orthorhombic Amm2) → FE (tetragonal P4mm) phase transition at $T_{tr}^{O\to T} = 204$°C and the FE (tetragonal P4mm) → PE (cubic Pm3m) phase transition at $T_{tr}^{T\to C} = 409$°C. The observed transition temperatures are in conformity with those reported for conventionally sintered KNN.[79–81] The maximum relative permittivity and loss tangent at $T_{tr}^{T\to C} = 409$°C were determined as $\varepsilon_r^{max} = 8247$ and tan($\delta$) = 0.8%, respectively, which are also comparable with reports in the literature for conventionally sintered KNN.[82]

We carried out Curie–Weiss analysis on the FE → PE transition at 409°C, which involved fitting of the $\varepsilon_r$ versus

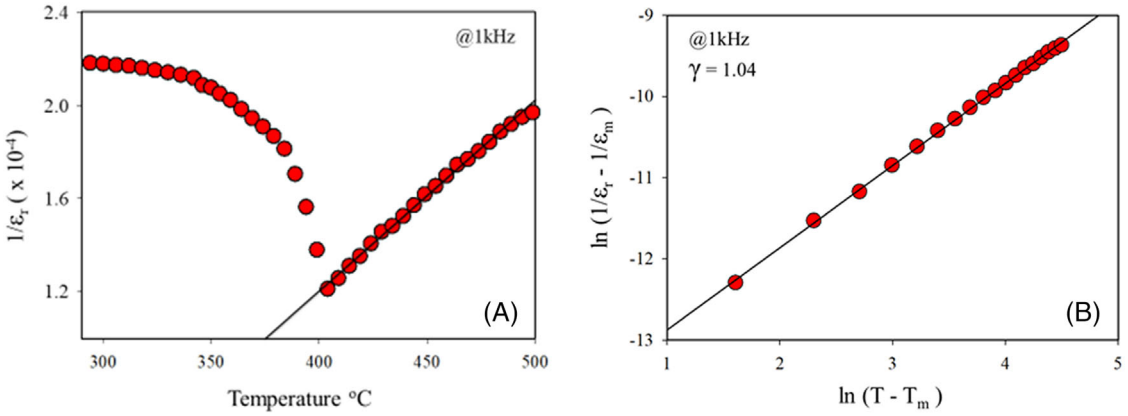


**FIGURE 7** Curie–Weiss analysis of dielectric response in the vicinity of $T_{tr} = 409°C$: (A) Curie–Weiss analysis gives the Curie–Weiss temperature ($\theta$) and constant ($C$) as $\theta = 375°C$ and $C = 3.1 \times 10^{-5}°C$, respectively. The transition at 409°C is first order since $T_{tr} > \theta$; (B) modified Curie–Weiss analysis gives the critical exponent as $\gamma = 1.04$, indicating the transition at 409°C is a normal ferroelectric transition

temperature data (see Figure 7A) to the inverted Curie–Weiss equation as per the study by Liu et al.[83]

$$\frac{1}{\varepsilon_r} = \frac{T-\theta}{C}, \tag{4}$$

where $T$ is the temperature (°C), $\theta$ is the Curie–Weiss temperature (°C), and $C$ is the Curie constant (°C). The said fit resulted in $C = 3.1 \times 10^{-5}°C$ and $\theta = 375°C$. Since $(T_{tr}^{t\to c} - \theta) \neq 0$, we conclude the FE → PE phase transition in the flash sintered KNN is first order. We analyzed the dielectric behavior (see Figure 7B) around $T_{tr}^{t\to c}$ further by using the modified Curie–Weiss law[29] according to

$$\frac{1}{\varepsilon_r} - \frac{1}{\varepsilon_r^{max}\frac{(T-T_{tr})^{\gamma}}{C^*}}, \tag{5}$$

where $\varepsilon_r^{max}$is the maximum dielectric constant at $T_{tr}^{t\to c}$, $C^*$ is the modified Curie constant, and $\gamma$ is the degree of diffuseness.[29] A normal ferroelectric has $\gamma = 1$, while an ideal relaxor ferroelectric has $\gamma = 2$.[29] Fitting our data to $\ln(1/\varepsilon_r - 1/\varepsilon_r^{max})$ versus $\ln(T-T_{tr})$ at 1 kHz resulted in $\gamma = 1.04$ for flash sintered KNN at $T_f = 667°C$ with $E = 100$ V/mm and 0.8 mA/mm$^2$ cut-off, suggesting normal ferroelectric behavior. We consider the slight deviation in $\gamma$ from unity as simple experimental scatter. As such, we conclude that FS of KNN at 100 V/mm has no effect on the ferroelectric character of the transition at 409°C.

We extended our analyses of the dielectric data and obtained the expansion coefficient of the quadratic polarization term in the Landau free energy functional ($\Delta G \approx \frac{1}{2}\alpha(T)P^2 + \cdots$.) as per Strukov and Levanyuk.[28]

$$\alpha(T) = -\frac{(T_{tr}-\theta)}{\varepsilon_o C} + \frac{(T-\theta)}{\varepsilon_o C}, \tag{6}$$

which, upon substitution of the experimentally determined values, becomes

$$\alpha(T) = [-1.239 + 0.036(T-\theta)] \times 10^7, \tag{7}$$

where the unit of $\alpha(T)$is $m/F$ in which the temperature is in degrees Celsius (°C).

## 4 | SUMMARY AND CONCLUSION

FS of KNN was accomplished under 100 V/mm dc electric field with 0.8 mA/mm$^2$ current density cut-off, and in the PPCC. Precipitous densification occurred over 662–670°C furnace temperature ($T_f$) range and in 60 s. The peak power absorption by KNN at 667°C was 55 mW/mm$^3$. The resultant KNN ceramic was of 98% density, with a microstructure that comprised ≤ 5-$\mu$m grain size.

The key finding of this study are as follows:

1. PPCC and the thin disc specimen geometry enable one to flash sinter KNN at higher electric fields, which results in lower FS temperatures (designated as furnace temperature in the manuscript). Also, the PPCC and the thin disc specimen geometry enable heat loss via conduction in addition to radiation, greatly reducing the possibility of thermal runaway.
2. A temperature rise of 147°C is estimated by using the black body radiation model, which is due to Joule heating, brings the specimen temperature to 809°C.
3. Joule heating alone cannot account for the densification of KNN via FS under 100 V/mm with a 0.8 mA/mm$^2$ because the FS time (60 s) is not accessible by thermal activation alone.

4. The local component of the applied electric field (a.k.a. the Lorentz field) is conjectured to couple with oxygen vacancies via the Lorentz force, enhancing the diffusion kinetics of densification in flash sintered KNN.
5. The low-frequency relaxation in dielectric permittivity in flash sintered KNN, which was attributed to GB space charge, is a remnant effect of FS.
6. The relaxation that $\varepsilon_r = 577$ at 100 kHz and represents the average relative permittivity of the KNN grains. The $\varepsilon_r$ is 4096 at 1 kHz that is because of the BLC effect.
7. The FE (tetragonal P4mm) → PE (cubic Pm3m) phase transition at $T_{tr}^{T\to C} = 409°C$ is first order for which $C = 3.1 \times 10^{-5}°C$ and $\theta = 375°C$.
8. The $\varepsilon_r^{max} = 8247$ at $T_{tr}^{T\to C} = 409°C$ to which corresponds a degree of diffuseness of 1.04, indicating normal ferroelectric behavior.

## ACKNOWLEDGMENTS

The authors gratefully acknowledge the financial support provided to this research program by the Scientific Research Projects Coordination Unit (SRPCU) of Selçuk University through contract# 18401032, and the Scientific Research Projects at Konya Technical University through contract# 191019035. The authors wish to thank Dr. H. Akyıldız and Dr. V. Kalem, both from Konya Technical University, for their technical feedback.

## CONFLICT OF INTEREST

The authors declare no conflict of interest.

## ORCID

*İlyas Şavklıyıldız* https://orcid.org/0000-0001-7903-9220

## REFERENCES

1. Safari A, Abazari M, Kerman K, Marandian-Hagh N, Akdogan EK. ($K_{0.44}$, $Na_{0.52}$, $Li_{0.04}$) ($Nb_{0.84}$, $Ta_{0.10}$, $Sb_{0.06}$)$O_3$ ferroelectric ceramics. IEEE Trans Ultrason Ferroelectr Freq Control. 2009;56(8):1586–94.
2. Saito Y, Takao H, Tani T, Nonoyama T, Takatori K, Homma T, et al. Lead-free piezoceramics. Nature. 2004;432(7013):84–7.
3. Takenaka T, Nagata H. *Present status of non-lead-based piezoelectric ceramics*. Key Eng Mater; 1999;157:57–64.
4. Baker D, Thomas P, Zhang N, Glazer A. A comprehensive study of the phase diagram of $K_xNa_{1-x}NbO_3$. Appl Phys Lett. 2009;95(9):091903.
5. Safari A, Akdogan EK. *Piezoelectric and acoustic materials for transducer applications*. Boston, MA: Springer Science & Business Media; 2008.
6. Akdoğan E, Kerman K, Abazari M, Safari A. Origin of high piezoelectric activity in ferroelectric ($K_{0.44}Na_{0.52}Li_{0.04}$)–($Nb_{0.84}Ta_{0.1}Sb_{0.06}$)$O_3$ ceramics. Appl Phys Lett. 2008;92(11):112908.
7. Abazari M, Akdoğan E, Safari A. Effect of manganese doping on remnant polarization and leakage current in ($K_{0.44}$,$Na_{0.52}$,$Li_{0.04}$)($Nb_{0.84}$,$Ta_{0.10}$,$Sb_{0.06}$)$O_3$ epitaxial thin films on Sr $TiO_3$. Appl Phys Lett. 2008;92(21):212903.
8. Guo Y, Kakimoto K-i, Ohsato H. Phase transitional behavior and piezoelectric properties of ($Na_{0.5}K_{0.50}$)$NbO_3$–$LiNbO_3$ ceramics. Appl Phys Lett. 2004;85(18):4121–3.
9. Zhang H, Li J, Chu W, Su Y, Qiao L. Effect of humidity and hydrogen on the promotion of indentation crack growth in lead-free ferroelectric ceramics. Mater Sci Eng B. 2010;167(3):147–52.
10. Mgbemere HE, Hinterstein M, Schneider GA. Structural phase transitions and electrical properties of ($K_xNa_{1-x}$) $NbO_3$-based ceramics modified with Mn. J Eur Ceram Soc. 2012;32(16):4341–52.
11. Li JF, Wang K, Zhang BP, Zhang LM. Ferroelectric and piezoelectric properties of fine-grained $Na_{0.5}K_{0.5}NbO_3$ lead-free piezoelectric ceramics prepared by spark plasma sintering. J Am Ceram Soc. 2006;89(2):706–9.
12. Jaeger R, Egerton L. Hot pressing of potassium-sodium niobates. J Am Ceram Soc. 1962;45(5):209–13.
13. Haertling G. Properties of hot-pressed ferroelectric alkali niobate ceramics. J Am Ceram Soc. 1967;50(6):329–30.
14. Cologna M, Rashkova B, Raj R. Flash sintering of nanograin zirconia in< 5 s at 850 C. J Am Ceram Soc. 2010;93(11):3556–59.
15. Yu M, Grasso S, Mckinnon R, Saunders T, Reece MJ. Review of flash sintering: materials, mechanisms and modelling. Adv Appl Ceram. 2017;116(1):24–60.
16. Biesuz M, Sglavo VM. Flash sintering of ceramics. J Eur Ceram Soc. 2019;39(2-3):115–43.
17. Becker MZe, Shomrat N, Tsur Y. Recent advances in mechanism research and methods for electric-field-assisted sintering of ceramics. Adv Mater. 2018;30(41):1706369.
18. Şavkliyildiz İ, Demir A. Flash sintering effect on PMN-PT ceramics. ECJSE. 8(2):793–99.
19. Akdoğan E, Şavklıyıldız İ, Biçer H, Paxton W, Toksoy F, Zhong Z, et al. Anomalous lattice expansion in yttria stabilized zirconia under simultaneous applied electric and thermal fields: A time-resolved in situ energy dispersive x-ray diffractometry study with an ultrahigh energy synchrotron probe. J Appl Phys. 2013;113(23):233503.
20. Wu Y, Su X, An G, Hong W. Dense Na0. 5K0. 5NbO3 ceramics produced by reactive flash sintering of $NaNbO_3$-$KNbO_3$ mixed powders. Scr Mater. 2020;174:49–52.
21. Corapcioglu G, Gulgun MA, Kisslinger K, Sturm S, Jha SK, Raj R. Microstructure and microchemistry of flash sintered $K_{0.5}Na_{0.5}NbO_3$. J Ceram Soc Japan. 2016;124(4):321–8.
22. Serrazina R, Ribeiro C, Costa ME, Pereira L, Vilarinho PM, Senos AM. Particle characteristics' influence on FLASH sintering of potassium sodium niobate: A relationship with conduction mechanisms. Materials. 2021;14(5):1321.
23. Rheinheimer W, Hoffmann MJ. Grain growth transitions of perovskite ceramics and their relationship to abnormal grain growth and bimodal microstructures. J Mater Sci. 2016;51(4):1756–65.
24. Dong Y, Chen IW. Onset criterion for flash sintering. J Am Ceram Soc. 2015;98(12):3624–7.
25. Dong Y, Chen IW. Predicting the onset of flash sintering. J Am Ceram Soc. 2015;98(8):2333–5.
26. Biçer H, Akdoğan EK, Şavklıyıldız İ, Haines C, Zhong Z, Tsakalakos T. Thermal expansion of nano–boron carbide under constant DC electric field: An in situ energy dispersive

X-ray diffraction study using a synchrotron probe. J Mater Res. 2020;35(1):90–7.
27. Von Hippel A. *Dielectrics and waves*. Norwood, MA: Artech House Inc.; 1995.
28. Strukov BA, Levanyuk AP. *Ferroelectric phenomena in crystals: physical foundations*. Cham: Springer Science & Business Media; 2012.
29. Du H, Zhou W, Luo F, Zhu D, Qu S, Pei Z. Phase structure, dielectric properties, relaxor behavior of $(K_{0.5}Na_{0.5})NbO_3$–$(Ba_{0.5}Sr_{0.5})$ $TiO_3$ lead-free solid solution for high temperature applications. J Appl Phys. 2009;105(12):124104.
30. Kim SW, Kim SG, Jung JI, Kang SJL, Chen IW. Enhanced grain boundary mobility in yttria-stabilized cubic zirconia under an electric current. J Am Ceram Soc. 2011;94(12):4231–8.
31. Biesuz M, Sglavo VM. Current-induced abnormal and oriented grain growth in corundum upon flash sintering. Scr Mater. 2018;150:82–6.
32. Lebrun JM, Raj R. A first report of photoemission in experiments related to flash sintering. J Am Ceram Soc. 2014;97(8):2427–30.
33. Jha SK, Terauds K, Lebrun J-M, Raj R. Beyond flash sintering in 3 mol% yttria stabilized zirconia. J Ceram Soc Japan. 2016;124(4):283–8.
34. Terauds K, Lebrun J-M, Lee H-H, Jeon T-Y, Lee S-H, Je JH, et al. Electroluminescence and the measurement of temperature during Stage III of flash sintering experiments. J Eur Ceram Soc. 2015;35(11):3195–9.
35. Biesuz M, Luchi P, Quaranta A, Martucci A, Sglavo VM. Photoemission during flash sintering: An interpretation based on thermal radiation. J Eur Ceram Soc. 2017;37(9):3125–30.
36. Serrazina R, Vilarinho PM, Senos AM, Pereira L, Reaney IM, Dean JS. Modelling the particle contact influence on the Joule heating and temperature distribution during FLASH sintering. J Eur Ceram Soc. 2020;40(4):1205–11.
37. Zhang S, Lee HJ, Ma C, Tan X. Sintering effect on microstructure and properties of (K, Na) NbO3 ceramics. J Am Ceram Soc. 2011;94(11):3659–65.
38. Du H, Li Z, Tang F, Qu S, Pei Z, Zhou W. Preparation and piezoelectric properties of $(K_{0.5}Na_{0.5})NbO_3$ lead-free piezoelectric ceramics with pressure-less sintering. Mater Sci Eng B. 2006;131(1-3):83–7.
39. Kumar P, Pattanaik M. Synthesis and characterizations of KNN ferroelectric ceramics near 50/50 MPB. Ceram Int. 2013;39(1):65–9.
40. Serrazina R, Senos AM, Pereira L, Dean JS, Reaney IM, Vilarinho PM. The role of particle contact in densification of FLASH sintered potassium sodium niobate. Eur J Inorg Chem. 2020;2020(39):3720–8.
41. Wu J, Xiao D, Zhu J. Potassium–sodium niobate lead-free piezoelectric ceramics: recent advances and perspectives. J Mater Sci: Mater Electron. 2015;26(12):9297–308.
42. Jha SK, Raj R. The effect of electric field on sintering and electrical conductivity of titania. J Am Ceram Soc. 2014;97(2):527–34.
43. Raj R. Joule heating during flash-sintering. J Eur Ceram Soc. 2012;32(10):2293–301.
44. Chaim R. Liquid film capillary mechanism for densification of ceramic powders during flash sintering. Materials. 2016;9(4):280.
45. Holland TB, Anselmi-Tamburini U, Quach DV, Tran TB, Mukherjee AK. Effects of local Joule heating during the field assisted sintering of ionic ceramics. J Eur Ceram Soc. 2012;32(14):3667–74.
46. Chen DJ, Mayo MJ. Rapid rate sintering of nanocrystalline ZrO2—3 mol% Y2O3. J Am Ceram Soc. 1996;79(4):906–12.
47. Yang D, Raj R, Conrad H. Enhanced sintering rate of zirconia (3Y-TZP) through the effect of a weak dc electric field on grain growth. J Am Ceram Soc. 2010;93(10):2935–7.
48. Charalambous H, Jha SK, Christian KH, Lay RT, Tsakalakos T. Flash sintering using controlled current ramp. J Eur Ceram Soc. 2018;38(10):3689–93.
49. Vikrant K, Wang H, Jana A, Wang H, García RE. Flash sintering incubation kinetics. Npj Comput Mater. 2020;6(1):1–8.
50. Lienhard I, John H. *A heat transfer textbook*. Cambridge, MA: Phlogiston Press; 2005.
51. Zhang Y, Shen B, Zhai J, Zeng H. New insight on sintering progress of KNN-based lead-free ceramics. J Am Ceram Soc. 2016;99(3):752–5.
52. Serrazina R, Dean JS, Reaney IM, Pereira L, Vilarinho PM, Senos AM. Mechanism of densification in low-temperature FLASH sintered lead free Potassium Sodium Niobate (KNN) piezoelectrics. J Mater Chem C. 2019;7(45):14334–41.
53. Khorrami GH, Kompany A, Zak AK. A facile sol–gel approach to synthesize KNN nanoparticles at low temperature. Mater Lett. 2013;110:172–5.
54. Özeren Y, Mensur-Alkoy E, Alkoy S. Sodium niobate particles with controlled morphology synthesized by hydrothermal method and their use as templates in KNN fibers. Adv Powder Technol. 2014;25(6):1825–33.
55. Hirvonen P, Fan Z, Ervasti MM, Harju A, Elder KR, Ala-Nissila T. Energetics and structure of grain boundary triple junctions in graphene. Sci Rep. 2017;7(1):1–14.
56. Czubayko U, Sursaeva V, Gottstein G, Shvindlerman L. Influence of triple junctions on grain boundary motion. Acta Mater. 1998;46(16):5863–71.
57. Johnson A, Voorhees PW. A phase-field model for grain growth with trijunction drag. Acta Mater. 2014;67:134–44.
58. Jaffe W, Cook WR, Jaffe H. *Piezoelectric ceramics*. New York: Academic Press; 1971.
59. Marion J, Hsueh C, Evans A. Liquid-phase sintering of ceramics. J Am Ceram Soc. 1987;70(10):708–13.
60. Yoon B, Yadav D, Ghose S, Sarin P, Raj R. On the synchronicity of flash sintering and phase transformation. J Am Ceram Soc. 2019;102(6):3110–6.
61. Morisaki N, Yoshida H, Tokunaga T, Sasaki K, Yamamoto T. Consolidation of undoped, monoclinic zirconia polycrystals by flash sintering. J Am Ceram Soc. 2017;100(9):3851–7.
62. Sinclair DC, Adams TB, Morrison FD, West AR. $CaCu_3$ $Ti_4O_{12}$: one-step internal barrier layer capacitor. Appl Phys Lett. 2002;80(12):2153–5.
63. Neumann H, Arlt G. Maxwell-wagner relaxation and degradation of $SrTiO_3$ and $BaTiO_3$ ceramics. Ferroelectrics. 1986;69(1):179–86.
64. Jayanthi S, Kutty T. Giant dielectrics from modified boundary layers in n-$BaTiO_3$ ceramics involving selective melting reactions of silver/glass composites at the grain boundaries. J Mater Sci: Mater Electron. 2005;16(5):269–79.
65. Ravi V, Kutty T. Field-dependent changeover from current- to voltage-limiting characteristics by non-linear n-type $BaTiO_3$ ceramics. J Mater Sci: Mater Electron. 1993;4(1):67–73.

66. Wang T, Hu J, Yang H, Jin L, Wei X, Li C, et al. Dielectric relaxation and Maxwell-Wagner interface polarization in $Nb_2O_5$ doped $0.65BiFeO_3$–$0.35\ BaTiO_3$ ceramics. J Appl Phys. 2017;121(8):084103.
67. Bi-Shiou C, Sin-Tah L, Duh J-G. EPR evidence for compensating defects in $BaTiO_3$ grain boundary barrier layer capacitors. Mater Chem Phys. 1990;24(3):239–45.
68. Wada N, Hiramatsu T, Tamura T, Sakabe Y. Investigation of grain boundaries influence on dielectric properties in fine-grained $BaTiO_3$ ceramics without the core–shell structure. Ceram Int. 2008;34(4):933–7.
69. Singh G, Tiwari V, Gupta P. Role of oxygen vacancies on relaxation and conduction behavior of $KNbO_3$ ceramic. J Appl Phys. 2010;107(6):064103.
70. Jha SK, Charalambous H, Wang H, Phuah XL, Mead C, Okasinski J, et al. In-situ observation of oxygen mobility and abnormal lattice expansion in ceria during flash sintering. Ceram Int. 2018;44(13):15362–9.
71. Zhang T-F, Tang X-G, Liu Q-X, Lu S-G, Jiang Y-P, Huang X-X, et al. Oxygen-vacancy-related relaxation and conduction behavior in $(Pb_{-x}Ba_x)(Zr_{0.95}Ti_{0.05})O_3$ ceramics. AIP Advances. 2014;4(10):107141.
72. Chiou B-S, Lin S-T, Duh J-G. The effect of sintering conditions on the grain growth of the $BaTiO_3$-based GBBL capacitors. J Mater Sci. 1988;23(11):3889-93.
73. Liu D, Cao Y, Liu J, Gao Y, Wang Y. Effect of oxygen partial pressure on temperature for onset of flash sintering 3YSZ. J Eur Ceram Soc. 2018;38(2):817–20.
74. Rafiq MA, Tkach A, Costa ME, Vilarinho PM. Defects and charge transport in Mn-doped $K_{0.5}Na_{0.5}NbO_3$ ceramics. PCCP. 2015;17(37):24403–11.
75. Guggenheim E. The conceptions of electrical potential difference between two phases and the individual activities of ions. J Phys Chem. 2002;33(6):842–9.
76. Guggenheim EA. *Thermodynamics-an advanced treatment for chemists and physicists*. Amsterdam: Nort-Holland; 1985.
77. Demirel Y. *Nonequilibrium thermodynamics: transport and rate processes in physical, chemical and biological systems*. Amsterdam: Elsevier; 2007.
78. Landau L, Lifshitz E. *Electrodynamics of continuous media. Vol. 8 (Course of theoretical physics)*. New York: Pergamon Press; 1984.
79. Patterson EA, Cann DP. Dielectric and piezoelectric properties of (K, Na)$NbO_3$-based piezoelectric ceramics. J Adv Dielectr. 2011;1(03):345–9.
80. Singh S, Negi J, Panwar N. Temperature dependent dielectric properties of (Na, K)$NbO_3$, near equimolar composition. Ceram Int. 2019;45(10):13067–71.
81. Xing J, Tan Z, Xie L, Jiang L, Yuan J, Chen Q, Wu J, Zhang W, Xiao D, Zhu J. Properties and structures of nonstoichiometric (K, Na)$NbO_3$-based lead-free ceramics. J Am Ceram Soc. 2018;101(4):1632–45.
82. Chen X, Yan X, Li X, Liu G, Sun J, Li X, et al. Excellent temperature stability on relative permittivity, and conductivity behavior of $K_{0.5}Na_{0.5}NbO_3$ based lead free ceramics. J Alloys Compd. 2018;762:697–705.
83. Liu L, Huang Y, Su C, Fang L, Wu M, Hu C, et al. Space-charge relaxation and electrical conduction in $K_{0.5}Na_{0.5}NbO_3$ at high temperatures. Appl Phys A. 2011;104(4):1047–51.

**How to cite this article:** Şavklıyıldız İ, Okur Ç, Akdoğan EK. Flash sintering and dielectric properties of $K_{0.5}Na_{0.5}NbO_3$. J Am Ceram Soc. 2022;105:469–480. https://doi.org/10.1111/jace.18119